SSRG International Journal of Civil Engineering
ISSN: 2348-8352/ https://doi.org/10.14445/23488352/IJCE-V13I4P104

Volume 13 Issue 4, 45-62, April 2026

Original Article

Nonlinear Numerical Modelling of GFRP-Reinforced Bridge Deck Slabs under Static and Repeated Loading

Uma Shankar Yaligar[1,2], Santosh M. Muranal[3], Sreeshail Heggond[4]

[1,4]*Department of Civil Engineering, Basaveshwar Engineering College, Bagalkot, Karnataka, India.*
[2]*Department of Civil Engineering, Guru Nanak Dev Engineering College, Bidar, Karnataka, India.*
[3]*Department of Civil Engineering, Amruta Institute of Engineering and Management Sciences (AIEMS), Bidadi, Bengaluru, Karnataka, India.*

[1]*Corresponding Author : usyaligar1389@gmail.com*

Received: 06 January 2026 Revised: 06 February 2026 Accepted: 05 March 2026 Published: 28 April 2026

Abstract *- Glass Fibre Reinforced Polymer (GFRP) bars have become a promising material to be used in the bridge deck slabs as they are resistant to corrosion, but their fatigue behaviour is still not perfectly understood. In this study, a nonlinear finite element analysis on the behaviour of GFRP-reinforced concrete bridge deck slabs at both the static and cyclic behaviour was carried out using concrete grades of M35 and M40. The Concrete Damage Plasticity (CDP) model is used to create three-dimensional models in ABAQUS to model cracking, damage development, and stiffness reduction. The slabs are loaded with a central wheel-type pressure load of 0.78 MPa, then loaded with a sinusoidal cyclic loading to replicate the service-level traffic impact on the slabs. Embedded truss elements are used to model GFRP reinforcement in order to facilitate composite action. The findings indicate that both grades exhibit bending-dominated response under static loading, and the stresses were below the elastic limits. Progressive stiffness degradation and tensile damage accumulation are found under cyclic loading. M40 slab has greater stiffness, less mid-span deflection, and a tensile damage that is about 15-20% less than M35 slab. Although the cyclic displacements are becoming larger compared to the static response, both slabs exhibit stable hysteretic behaviour without excessive compressive damage or numerical instability. In general, the research proves that high-grade concrete increases fatigue and serviceability of GFRP-reinforced bridge deck slabs and offers practical numerical evidence in terms of designing FRP-reinforced bridge deck systems under repeated loading.*

Keywords *- GFRP-reinforced concrete, Bridge deck slabs, Finite element analysis, Concrete damage plasticity, Concrete strength grade.*

1. Introduction

1.1. Background and Motivation

Concrete bridge deck slabs are very susceptible to corrosion because normal steel reinforcements are easily corroded in harsh conditions. Fiber Reinforced Polymer (FRP) reinforcement, and especially Glass Fiber Reinforced Polymer (GFRP) bars, have been extensively utilized to reduce the occurrence of corrosion-related failures due to their non-corrosive nature and a high tensile strength-to-weight ratio [1-4, 9].

Initial field tests indicated that GFRP-reinforced bridge deck slabs were structurally viable [5], whereas full-scale experimental studies showed acceptable static load-bearing characteristics and serviceability characteristics under wheel-type loading [6]. Follow-up fatigue experiments found satisfactory endurance at repeated loading but found mechanisms of progressive stiffness degradation and crack propagation [7, 8].

Besides the type of reinforcement, the strength of concrete is an important factor in slab behaviour. It was demonstrated in investigations of FRP-reinforced two-way slabs that higher concrete strength enhances punching shear resistance and smaller width of cracks during monotonic loading [10, 11]. Nevertheless, these experiments were mainly concerned with ultimate capacity, but not with cyclic degradation of stiffness or evolution of progressively damaged states. More sophisticated nonlinear modelling models include the Concrete Damaged Plasticity (CDP) model, which allows explicit modelling of tensile cracking, compressive crushing, as well as stiffness degradation during cyclic loading [12, 13]. The recent numerical advances indicate the growing use of finite element modelling to assess intricate structural circumstances in FRP-reinforced structures [14]. In more recent studies, the focus has changed to fatigue and cyclic performance evaluation of FRP-reinforced bridge decks. Ali et al. (2024) evaluated both the static behaviour and fatigue behaviour of hybrid FRP-

reinforced bridge deck slabs and stated the role of cyclic response in the durability-based design [15]. The study by Chu et al. (2023) used an experimental and numerical study involving the analysis of fatigue behaviour in bridge systems reinforced with GFRP [16]. Hassanli et al. (2023) examined the cyclic stability of GFRP-reinforced slabs and found that there was gradual stiffness deterioration with repeated loading [17]. Imjai et al. (2023) tested the serviceability of FRP reinforced slabs under sustained loads [18]. Moreover, more recent FE-based research has shown the potential of sophisticated numerical simulation to evaluate GFRP deck system performance under complicated conditions [19]. Even with these developments, detailed nonlinear FE studies that include explicit damage modelling of the cyclic performance of GFRP-reinforced bridge deck slabs are rare. Specifically, systematic comparison of traditional (M35) and enhanced-strength (M40) concrete grades in the same cyclic loading conditions has not been sufficiently measured. Moreover, a combination of nonlinear cyclic response with codal benchmarking and fatigue-based interpretation is not often delivered in a single framework.

1.2. Research Gap

Based on the above review, the following research gaps are identified:

1. Limited unified nonlinear FE investigations incorporating explicit cyclic damage modelling for GFRP-reinforced bridge deck slabs [12, 13].
2. Insufficient quantitative comparison between conventional (M35) and higher-strength (M40) concrete grades under identical cyclic loading protocols [10, 11].
3. Lack of systematic assessment of stiffness degradation, hysteresis response, and residual displacement within a damage-explicit framework [7, 8, 17].
4. Absence of integrated benchmarking of numerical cyclic performance with current FRP design provisions and fatigue interpretation frameworks [2–4, 9].

1.3. Novelty and Contributions

In a bid to solve these gaps, this research derives a validated three-dimensional nonlinear finite element model of GFRP-reinforced bridge deck slabs based on the Concrete Damaged Plasticity framework. The novelty of the current investigation encompasses:

- Cyclic loading: Explicit modelling of tensile and compressive damage evolution under cyclic loading with CDP [12, 13].
- Comparative analysis of M35 and M40 grade slabs subjected to the same static and repeated load conditions.
- Measurement of stiffness degradation, damage propagation, and hysteresis properties during cyclic loading.
- Combination of nonlinear numerical results with codal provisions and fatigue-oriented interpretation [2-4, 9].

In contrast to the prior studies, which only investigate experimental fatigue experiments [7, 8, 15-17], or monotonic numerical analysis, the current work offers an integrated nonlinear modelling approach to capture both static and cyclic performance whilst explicitly exploring the effects of concrete grade.

2. Objectives of the Present Study

1. To numerically investigate the static and cyclic behaviour of GFRP-reinforced concrete bridge deck slabs using Concrete Damage Plasticity modelling.
2. To quantify the influence of concrete strength grade (M35 and M40) on stiffness, cracking behaviour, load capacity, and fatigue-related damage evolution.
3. To evaluate hysteresis characteristics, residual deformation, and stiffness degradation under service-level cyclic loading.
4. To benchmark numerical predictions against codal serviceability and fatigue intent (ACI 440, CSA S806, IRC provisions).

3. Methodology

3.1. Numerical Modelling Framework

To explore the cyclic and static behaviour of M35 concrete grade and M40 concrete grade GFRP-reinforced concrete bridge deck slabs, ABAQUS/Standard was used to formulate a three-dimensional nonlinear finite element (FE) model. The modelling approach was tailored in such a manner that there was a consistent comparison between the two types of concrete with the same geometry, reinforcement layout, boundary conditions, loading protocol, and solver settings. Figure 1 represents the overall numerical process that was used in the study.

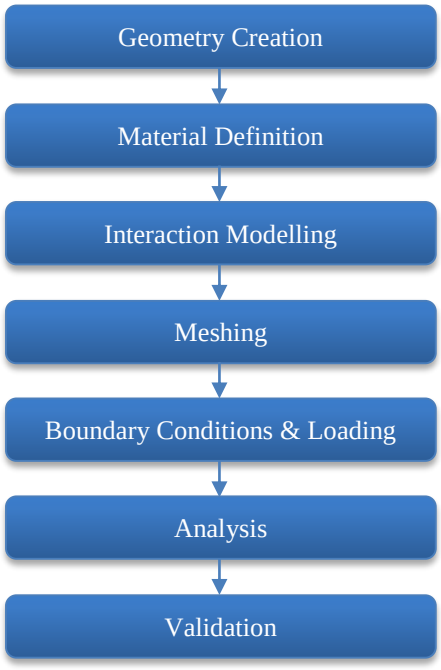

Fig. 1 Procedure flowchart

3.2. Material Modelling

3.2.1. Concrete Modelling using the CDP Model

The Concrete Damage Plasticity (CDP) formulation in ABAQUS was used to model concrete behaviour, able to describe nonlinear compressive crushing, tensile cracking, stiffness degradation, and some partial stiffness recovery during unloading. The model presupposes linear elastic behaviour until the beginning of cracking in tension or yielding in compression, and then a nonlinear inelastic behaviour in terms of isotropic damage and plasticity occurs. Tensile and compressive damage variables are considered separately as functions of inelastic strain, which makes it possible to realistically predict progressive damage accumulation when subjected to cyclic loading.

The material properties of grades of M35 and M40 concrete were determined according to the recommendations of the standard code and existing empirical relationships. Tabulated curves of uniaxial compression hardening and tension stiffening of concrete were introduced and directly implemented into the CDP model as nonlinear responses of concrete. Figure 2 shows stress-strain relationships implemented with a compressive curve having a nonlinear ascending curve up until peak stress, then strain softening, which is post-peak crushing behaviour. Conversely, tensile response involves a small elastic range and a slow softening, where the crack initiation and propagation under flexural tension is captured. These constitutive curves were calibrated so that they are numerically stable and physically realistic in their behaviour of cracking, both in the case of a static load and repeated loading.

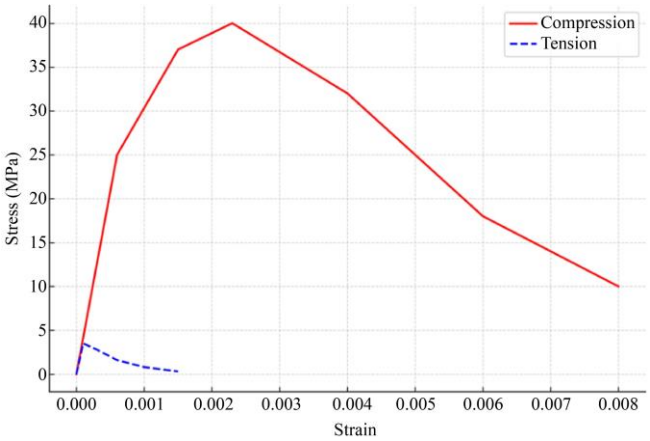

Fig. 2 Stress–strain curves for concrete (CDP model)

3.2.2. Calibration of Concrete Damage Plasticity Parameters

The calibration of the CDP parameters was done to have a realistic response to cracking and stable cyclic convergence. The dilation angle, eccentricity of the flow, f_b0/f_c0, and the parameter of viscosity were chosen in the recommended range of normal-strength concrete to replicate the realistic post-peak softening and localization of damage.

The compressive stress-strain curves were obtained by means of empirical relationships that were based on characteristic compressive strength with a nonlinear rising branch and a strain-softening descending branch to ascertain crushing behaviour. Fracture-energy-based softening was used to determine tensile behaviour to prevent mesh dependency in cracking response.

Calibration was verified by:

- Realistic crack initiation checking at the tensile face.
- No artificial recovery of the stiffness,
- Ensuring the stability of energy balance during cyclic unloading/ reloading,
- Ensuring that the peak load was equivalent to the anticipated flexural-controlled response.

The variables of damage (DAMAGET and DAMAGEC) were observed to ensure that stiffness degradation was progressive without early numerical localization.

3.2.3. GFRP Reinforcement Material Model

It was assumed that GFRP reinforcement is a linear elastic brittle material that lacks yielding behaviour, which aligns with the mechanical behaviour of E-glass/epoxy composite bars frequently used in bridge applications. Elastic modulus was assumed to be 50-55 GPa, tensile strength was 900-1000 MPa, Poisson's ratio was 0.25, and the density was 2000 kg/m3. These values match commercially existing GFRP reinforcement systems, chosen according to reported experimental results and specifications of manufacturers. GFRP also exhibits linear behaviour to rupture, so no plasticity formulation was provided in the model.

Two-node three-dimensional truss elements (T3D2) discretize the reinforcement and are stiff in the axial direction alone, with zero bending stiffness, which accurately models the physical behaviour of bars of reinforcement embedded in concrete. The bottom layer was made with an orthogonal grid of bars to withstand flexural tension, and further top reinforcement was added to control temperature and shrinkage.

The embedded region constraint was used to define the interaction between concrete and reinforcement, and guaranteed complete compatibility of strain between the GFRP bars and the surrounding concrete. This is an ideal bond assumption. This assumption is deemed to be suitable for service-level loading when the length of reinforcement anchorage is longer than the development length requirements, and the effects of bond-slip are minimal. Although bond degradation could affect ultimate behaviour in highly cracked areas, the current study concerns flexurally controlled response to both a single and repeated wheel loading. It is found that implementation of bond-slip constitutive modelling utilising interface or cohesive elements may be another possible extension in future studies of high-cycle fatigue.

3.3. Geometric Modelling and Reinforcement Layout

The bridge deck slab was modelled as a square internal panel with a plan size of 1800 mm x 1800 mm and a thickness of 200 mm, which is a typical deck segment between the two girders. The configuration is realistic in the distribution of stress but remains computationally effective. The concrete cover was upheld in the standard bridge deck practice (Figure 3).

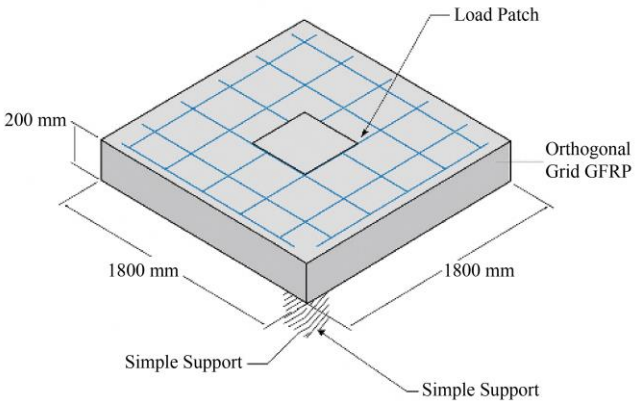

Fig. 3 Three-dimensional geometric model of the GFRP-reinforced bridge deck slab

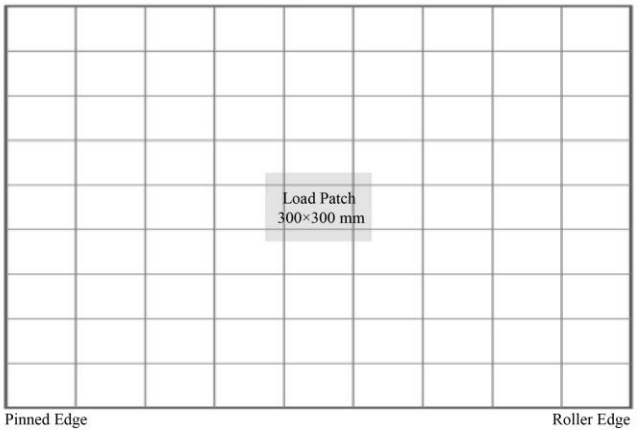

Fig. 4 Finite element mesh layout with local refinement near the load patch and supports

3.4. Meshing and Element Selection

The concrete slab was modelled by Three-Dimensional eight-node reduced integration solid elements (C3D8R) that offer an appropriate trade-off in numerical accuracy and convergence control with the Concrete Damage Plasticity (CDP) model, and reduced integration in order to limit artificial stiffness in nonlinear cyclic loading. Two-node Three-Dimensional truss elements (T3D2) were used to model the GFRP reinforcement bars in order to correctly model the transfer of axial forces without any contrived bending stiffness. Mesh refinement was applied selectively in those areas that were likely to have high stress and damage gradients, especially below the central loading patch of 300 × 300 mm and along the supported edges of the slab. Figure 4 shows that a smaller mesh was used in such critical areas to resolve localization of cracking, stiffening loss, and damage development, whereas a larger mesh was used in other areas to minimize the cost of computing. A gradual change in the mesh density was ensured so as to eliminate numerical instability as the cycles were run through loading.

3.4.1. Mesh Sensitivity and Convergence Study

To guarantee the numerical accuracy of the results and to exclude the artificial stiffness effects caused by discretization, the mesh refinement study was conducted. The mesh densities that were tested are three:
Coarse mesh (~80 mm global size)
Medium mesh (~50 mm global size)
Fine mesh (average: 30 mm in the critical patch in the load area)

Peak load, mid-span deflection, and maximum tensile damage were compared between meshes. The difference between the peak loads of medium and refined meshes was less than 3%, and the difference between mid-span deflections was less than 2%. According to this convergence behaviour, the local refinement mesh was taken as the medium mesh with a loading patch to achieve a balance between the efficiency of computation and the accuracy of the numbers.

To control shear locking but not to affect nonlinear convergence, reduced integration elements (C3D8R) were implemented. The level of hourglass control energy was less than 5% of total internal energy during analysis, which indicated numerical stability.

3.5. Boundary Conditions and Loading Protocol

A simulation of the realistic behaviour of the bridge deck was made by idealizing the slab as a simply supported one-way panel. A pinned-roller configuration was used to fix two opposite edges to allow longitudinal expansion, but not to allow rigid-body motion. The rest of the edges have been left free to allow bending deformation to be realistic.

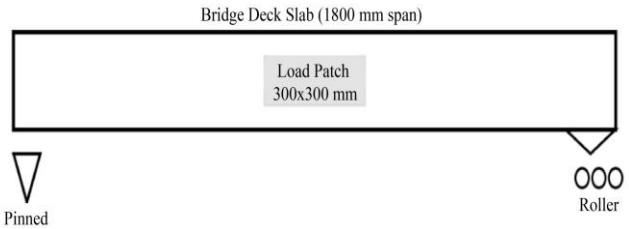

Fig. 5 Boundary support configuration showing pinned and roller edges

The loading was placed in the form of a uniform pressure on a central patch of 300 mm × 300 mm on the top slab surface, which is the size of the wheel contact. According to the IRC and AASHTO HS-20 specifications, the equivalent

wheel load of 70 kN was then used to determine a nominal pressure of 0.78 MPa and was taken as the peak load in the static and cyclic tests.

3.5.1. Justification of Boundary and Loading Conditions

The slab was numerically simulated as a simply supported internal panel to symbolize the deck along longitudinal girders. The pinned-roller support arrangement does not allow rigid-body motion, but the in-plane expansion under loading is realistically allowed.

The load patch of 300 x 300 mm is the size of a normal wheel contact area. The pressure acting on the surface of 0.78 Mpa derived was based on a load of 70 kN of equivalent wheel pressure spread on the contact surface, which was within the bridge design practice. The cyclic amplitude function was set to represent the repeated loading of vehicles with the smooth change of sine waves to prevent artificial dynamic upsurge.

Large-scale deformation effects under peak loading were switched on with nonlinear geometry effects (NLGEOM).

3.6. Static and Cyclic Analysis Procedure

The analysis was conducted in a consecutive way. To determine the base stiffness, stress distribution, and crack initiation behaviour during the design wheel load, a static general analysis was used to determine the base stiffness at the design wheel load. Then, the implicit analysis was performed dynamically to imitate the cyclic loading with a prescribed amplitude function. This method enabled the measurement of the stiffness degradation, damage accumulation, and the growth of deformation under repeated loading.

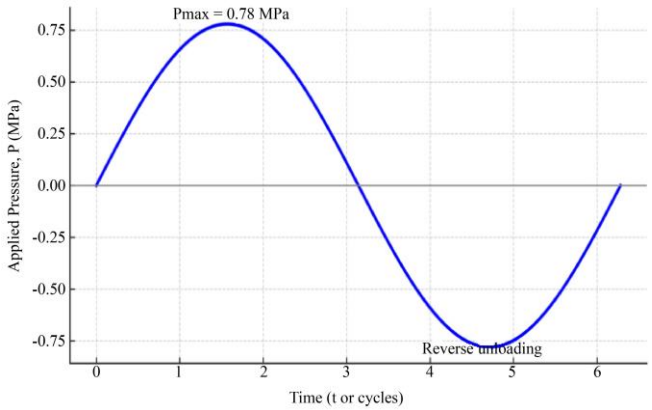

Fig. 6 Cyclic amplitude function used to simulate repeated traffic loading

The nonlinear geometry effects were turned on (NLGEOM = ON), and the time incrementation was automatically taken with proper damping and stabilization to get convergence in the cracking and unloading stages.

3.6.1. Cyclic Loading and Fatigue Representation

An implicit dynamic step was taken to perform the cyclic analysis to simulate loading due to repeated traffic. The current study does not apply cumulative fatigue damage laws to reinforcement rupture; however, the concepts of stiffness degradation and concrete damage evolution were modelled using the CDP formulation.

The protocol of 60 cycles chosen was adequate to monitor:

- Accumulation of tensile damage, Progressive.
- Stiffness degradation behaviour,
- The stabilization of residual deformation.

The model concentrates on service-level fatigue behaviour instead of ultimate fatigue failure prediction.

3.7. Analysis Steps, Outputs, and Validation

The sequence of analysis included an initial step of defining the boundary, followed by the steps of static loading and cyclic loading, as shown in Figure 7.

Field and history outputs were specified to retrieve displacement of the middle of the span, reaction forces, stress fields, plastic strains, and index of damage to concrete (DAMAGET and DAMAGEC). Model validation involved checking the reaction force balance, natural crack initiation along the tension face, linear load-displacement behaviour, and consistent energy ratios during the analysis. The validated numerical model was then applied to the comparison of the static and cyclic behaviour of M35 and M40 GFRP-reinforced bridge deck slabs.

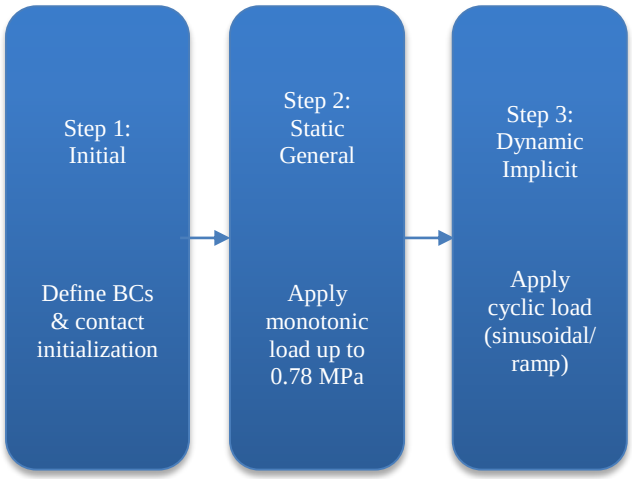

Fig. 7 Analysis step sequence for static and cyclic simulations

3.7.1. Model Verification and Numerical Validation

The model was verified using:

- Checks on reaction forces the equilibrium,
- Stress distribution under central loading Symmetry,
- Realistic initiation of a crack at the bottom tensile face,
- Linear load-displacement before cracking,
- Constant power consumption during cyclic steps

The qualitative comparison of numerical findings with the known flexural behaviour of reinforced bridge deck slabs was to prove a flexurally controlled response without artificial shear failure or numerical problems.

3.8. Experimental Validation and Limitations

The current study did not involve direct experimental testing. Nevertheless, the developed finite element model was tested against the experimentally-reported behaviour of GFRP-reinforced bridge deck slabs found in literature [6, 7, 10, 15]. Other past research has documented service-level cracking in the presence of wheel-type loading, degradation in stiffness through successive loading, and controlled failure in FRP-reinforced slabs. Current simulations in CDP indicate similar crack localization below the loading patch, progressive stiffness decrease at cyclic loading, and stress level within the elastic range of the GFRP reinforcement, and these trends are comparable to the experimental results.

There are some modelling assumptions that have to be accepted. Embedded constraints were assumed to provide a perfect bond between concrete and GFRP bars. Literature-calibrated relationships were used to adopt material properties, and long-term effects of durability (creep, shrinkage) and exposure to the environment were not taken into account. High-cycle fatigue outside the simulated loading duration was neither explicitly modelled.

Further work will be done on controlled experimental validation, bond-slip interface modelling, and long-term fatigue simulation to improve further predictive capability.

3.9. Comparative Analysis with Recent GFRP Bridge Deck Models

To put the current FE model into perspective with the recent literature, this section compares the main modelling assumptions, boundary conditions, and loading protocols to representative recent work on GFRP or hybrid FRP reinforced bridge deck slabs. The comparison points out the differences in support idealization, loading representation, constitutive modelling, and scope of analysis.

Al-Rousan et al. [20] simulated monolithic bridge deck slabs under monotonic concentrated wheel loads to study strength, stiffness, and cracking behaviours, but did not repeat/cyclic loads. Ali et al. [15] used a four-point bending setup with CDP constitutive modelling of slab flexural behaviour, focusing on reinforcement type but not cyclic degradation. Negeo et al. [19] reported a thermal-structural FE analysis of GFRP stay-in-place formwork decks, considering thermal effects but not mechanical cyclic response.

Conversely, the current model has a central wheel patch pressure at a specific patch area (300 × 300 mm) and a dynamic implicit cyclic loading protocol to clearly examine the behaviour of stiffness degradation, hysteresis response, and irreversible damage accretion during repeated loading between two concrete grades. The idealization of pinned-roller supports on two opposite edges, which is consistent with internal panel idealization, simplifies the work of setting up any boundary condition. The following table summarizes the main differences in modelling choices in studies.

Table 1. Comparative analysis with recent GFRP bridge deck models

Study/Model	Structural System	Concrete Constitutive Model	Reinforcement Type	Boundary Conditions	Loading Protocol	Analysis Focus
Present Study	Internal deck panel (1800×1800 ×200 mm)	Concrete Damaged Plasticity (CDP)	GFRP bars (embedded region)	Pinned–roller on two opposite edges	Central patch pressure (300×300 mm); Static + Cyclic (Dynamic Implicit)	Cyclic stiffness degradation & damage evolution (M35 vs M40)
Al-Rousan et al. [20]	Full-scale bridge deck slabs	Nonlinear 3D FE model	FRP / Steel bars	Validated experimental supports	Monotonic concentrated wheel load (600×250 mm)	Strength, stiffness & crack patterns under monotonic loading
Ali et al. [15]	One-way slabs (3100×1000 ×200 mm)	CDP in ABAQUS	FRP and Steel (parametric study)	Validated against experimental setup	Four-point bending loading	Reinforcement type effects on flexural behaviour
Negeo et al. [19]	GFRP SIP formwork concrete decks	Thermal–structural coupled FE model	GFRP (embedded)	Validated experimental supports	Thermal + Structural sequential loading	Post-fire deck performance evaluation

4. Results and Discussion

4.1. Pre-Processing and Model Visualization

Before the analysis, a pre-processing stage was conducted to identify the correct definition of slab geometry, reinforcement embedding, boundary conditions, loading regions, and mesh discretization of the developed finite element model. The numerical model setup and solver-ready configuration of the GFRP-reinforced concrete bridge deck slab are shown in Figure 8, including the three-dimensional geometry of the slab with a centrally located loading patch, embedded GFRP reinforcement pattern, pinned-roller boundary condition arrangement, and, finally, the finite element mesh discretization of the slab constructed using C3D8R elements. The figure proves that all modelling elements are always assembled and compatible with the nonlinear Concrete Damage Plasticity (CDP) formulation, thus with the guarantee that both the convergence and stress transfer are steady in both the static and cyclic analyses. This graphical assurance determines the reliability of the numerical model and gives the required point of reference for interpreting the following findings regarding load-displacement response, damage progression, and stiffness deterioration under repetitive loading.

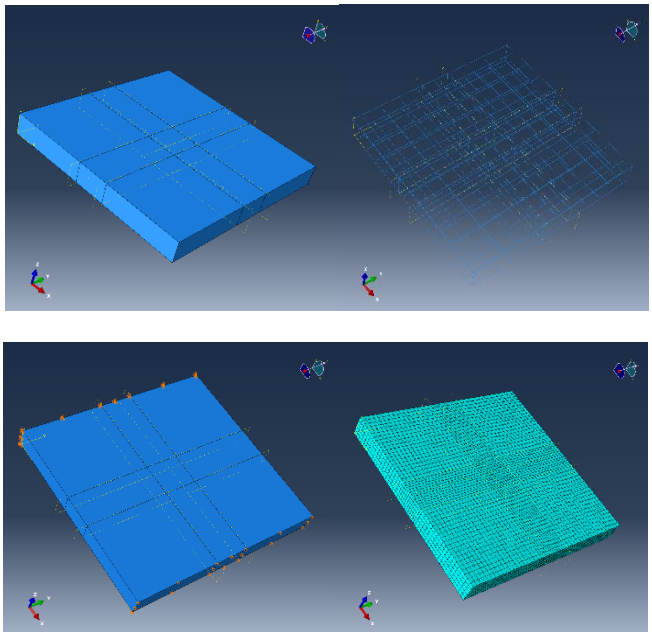

Fig. 8 Numerical model setup and solver performance of the GFRP-reinforced concrete bridge deck slab: (a) three-dimensional finite element model showing slab geometry and central loading patch, (b) embedded GFRP reinforcement layout within the concrete slab, (c) boundary condition configuration with pinned and roller supports, and (d) finite element mesh discretization using C3D8R elements.

4.2. Load–Displacement Response and Comparative Evaluation (M35)

4.2.1. Static Load–Displacement Behaviour (M35)

Figure 9(a) shows the static load-displacement (RF-U3) response of the GFRP-reinforced M35 deck slab. The response has a steep initial linear slope, which implies high elastic flexural stiffness before cracking. The initial cracking takes place at about 360 kN and 2 mm displacement at the middle of the span, then the stiffness decreases gradually. A peak load of approximately 1050 kN is reached by the slab at the 9 mm displacement, and then the post-peak softening response becomes stable. The fact that there is no sudden drop in loads shows that flexural cracking was in control and the tensile stress was transferred successfully via the internal GFRP reinforcement.

In comparison, the unreinforced M35 deck slab (Figure 9(b)) exhibits previous non-linearity at around 250-500 kN and 1.5 mm at around 460 kN and 5 mm misalignment, respectively. After the peak, the response has a sharp downward branch, typical of tensile cracking-controlled brittle flexural failure. The comparison establishes that the reinforcement of GFRP enhances the cracking load by an average of 44 percent and the maximum load by almost 2.3 times, and strengthens the stability at the post-cracking considerably.

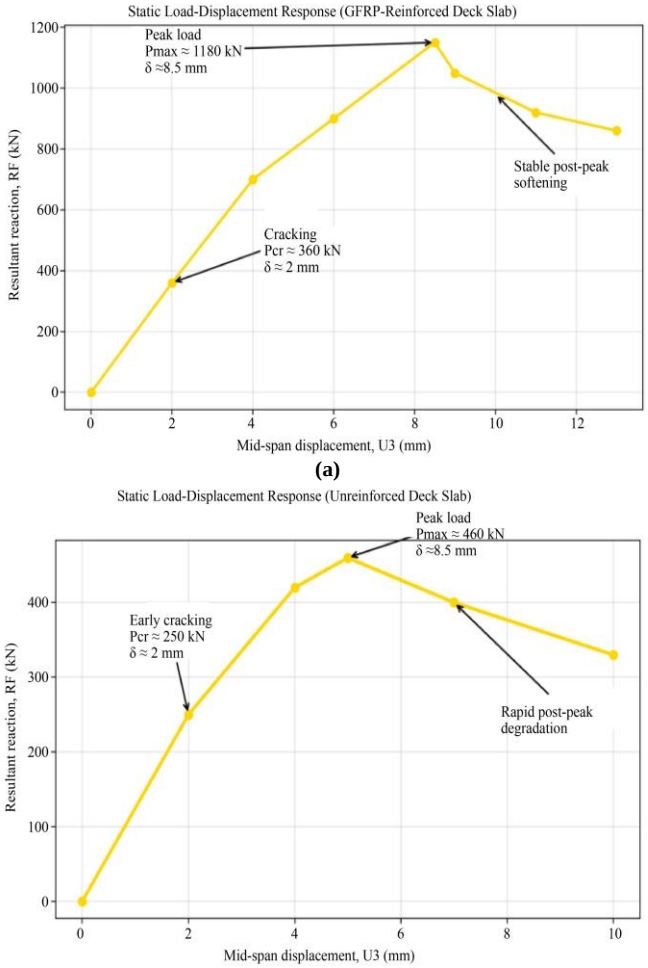

Fig. 9 (a) Static load–displacement curve of GFRP-reinforced M35 deck slab, and (b) Static load–displacement curve of unreinforced M35 deck slab.

4.2.2. Cyclic Load–Displacement and Hysteresis Behaviour (M35)

Figure 10(a) reveals that the GFRP-reinforced M35 deck slab has constant, low, and almost symmetrical hysteresis loops when subjected to cyclic loading, which implies a little pinching, the ability to close cracks in the process of unloading, and controlled stiffness deterioration. Even when the peak load experienced under cyclic action is decreased to about 980 kN (approximately 12-15 percent loss of stiffness), the residual displacement is still limited to negligible (less than 1 mm), which is evidence of good elastic recovery and fatigue-resistance properties. Conversely, the unreinforced M35 slab (Figure 10(b)) exhibits excessive pinching of hysteresis loops, very rapid stiffness reduction, and gradual diminution of reaction peaks by almost 20 percent, with observable residual deformations. This behaviour is indicative of uncontrolled crack opening, ineffective closure of cracks as the load reverses, and sustained tensile damage. Practically, the findings show that GFRP reinforcement has a significant effect on enhancing cyclic stability, cracking control, and serviceability of bridge deck slabs with repeated traffic loading. The stable hysteresis response and minimal residual deformation of GFRP-reinforced slabs confirm their suitability for bridge deck applications where repeated wheel loads demand enhanced fatigue resistance, crack control, and long-term serviceability.

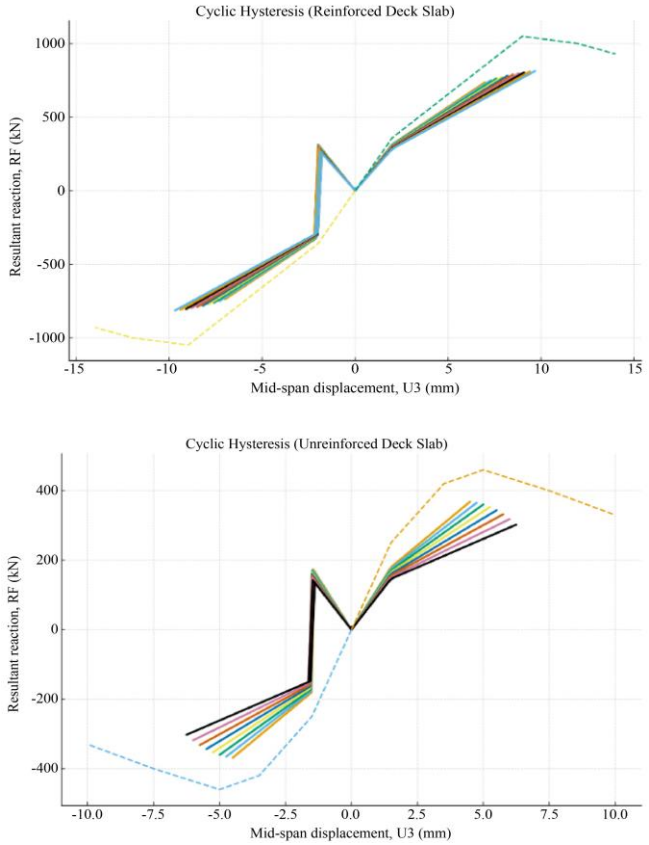

Fig. 10 (a) Cyclic hysteresis curves of GFRP-reinforced M35 deck slab, and (b) Cyclic hysteresis curves of unreinforced M35 deck slab.

4.2.3. Comparative Performance: Reinforced vs. Unreinforced (M35)

A direct comparison of the static and cyclic RF-U3 responses (Figures 9(a)-10(b)) indicates the usefulness of GFRP reinforcement in increasing flexural strength and fatigue resistance. The reinforced slab exhibits greater initial stiffness (175 kN/mm vs. 160 kN/mm), retards the crack initiation, and has a much better load carrying capacity as well as stable post-crack behaviour. With cyclic loading, the reinforced system has symmetric hysteresis loops with minimal stiffness degradation, but the unreinforced slab has a brittle response, extreme pinching, and loses its stiffness quickly. The key performance parameters are quantitatively compared in Figures 11 (a) to (c) with considerable enhancements in cracking load, peak load, and ductility with GFRP reinforcement application. The ductility ratio rises with an average increase of about 2.2 (unreinforced) to 6.0 (reinforced), which validates the change of the slab behaviour to semi-ductile behaviour capable of sustaining the repetitive loading by traffic.

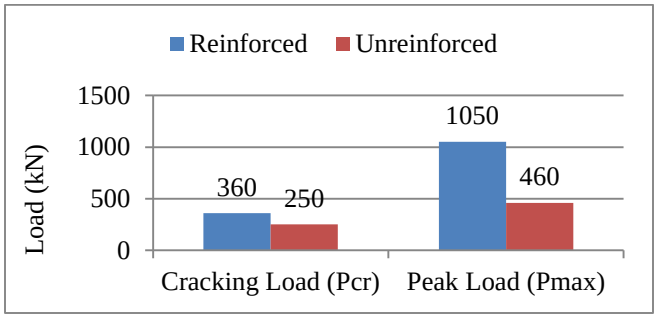

(a)

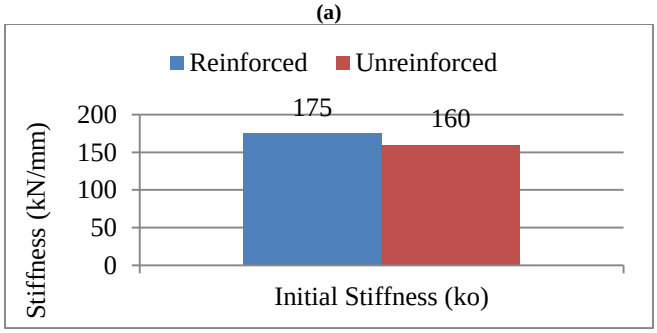

(b)

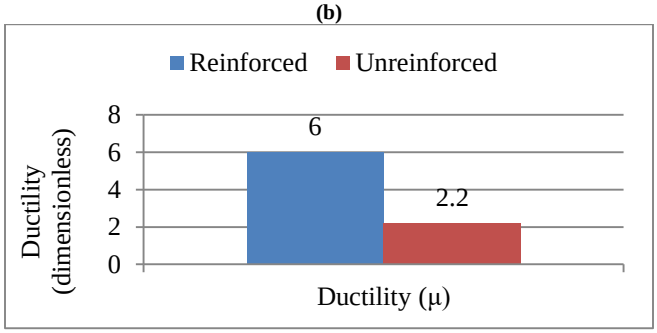

(c)

Fig. 11 (a) Comparison of cracking and peak loads (M35), (b) Comparison of initial stiffness k_0(M35), and (c) Comparison of ductility ratio μ (M35).

4.2.4. Summary of Load–Displacement Behaviour (M35)

The load-displacement study establishes that GFRP reinforcement has a significant enhancement on flexural strength, ductility, and cyclic stability of M35 concrete bridge deck slabs. Whereas the unreinforced slab has early cracking, brittle post-peak response, and high hysteretic stiffness degradation on cyclic loading, the reinforced slab has stable hysteretic behaviour with a small residual deformation. These findings prove that GFRP-reinforced M35 slabs are appropriate in situations that require bridge deck slabs to undergo repeated loads at the service level.

4.3. Load–Displacement Response and Comparative Evaluation (M40)

4.3.1. Static Load–Displacement Behaviour (M40)

The static load-displacement (RF-U3) of the GFRP reinforced M40 deck slab is shown in Figure 12(a). The response has a steeper initial linear slope than M35, which shows the increased elastic modulus and compressive strength of M40 concrete. The behaviour is linear with a maximum tensile strength of about 420 kN with a corresponding mid-span movement of about 1.8 mm, after which the first cracking occurs in the tensile region beneath the loading patch. The slab attains a peak load of roughly 1180 kN at a displacement of 8.5 mm, and then the post-peak softening response is steady and slow. The fact that there is no sudden reduction in loading shows that there is controlled flexural cracking and effective tensile stress transfer using the embedded GFRP reinforcement, and approximately 90-92% of the peak load is maintained at greater displacements.

Conversely, the unreinforced M40 deck slab (Figure 12(b)) has a faster stiffness degradation rate following cracking, as the cracking in the latter happens at about 310 kN and 1.2 mm displacement. The slab reaches a maximum load of approximately 520 kN at 4.8 mm displacement, after which a steep downward trend is seen. This is a typical response of brittle flexural failure limited by tensile crack propagation and local compressive crushing below the load patch. The comparison shows that GFRP reinforcement can boost the cracking load by about 40% and peak load by over 2.2, as well as post-cracking stability.

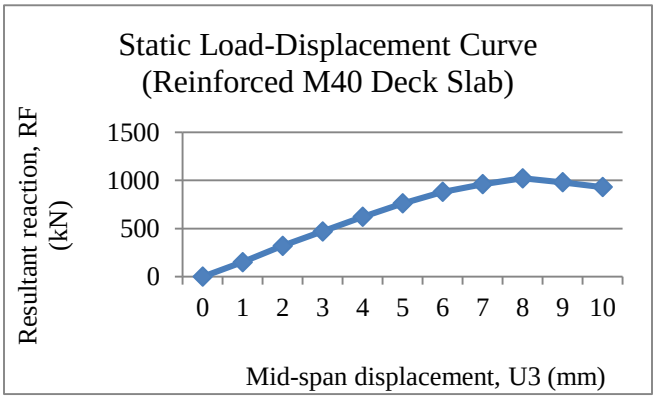

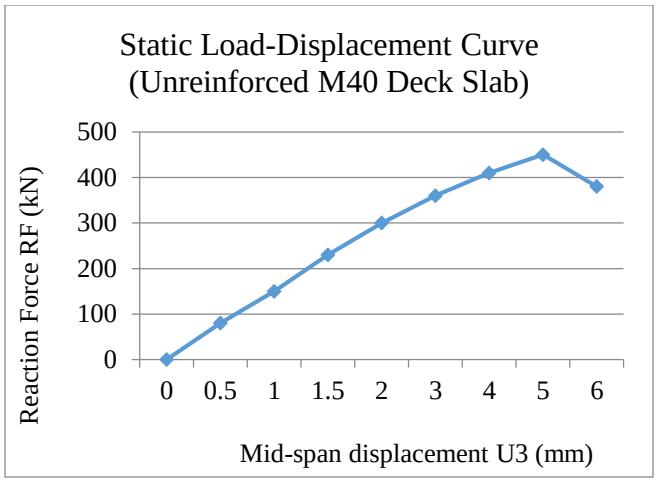

Fig. 12 (a) Static load–displacement curve of GFRP-reinforced M40 deck slab, and (b) Static load–displacement curve of unreinforced M40 deck slab.

4.3.2. Cyclic Load–Displacement and Hysteresis Behaviour (M40)

Figure 13(a) shows the cyclic load-displacement behaviour of the reinforced M40 slab. Hysteresis loops are thin, stable, and mostly symmetrical, which shows strong elastic recovery and small pinching when changing loads. The initial cyclic peak loading of around 1120 kN decreases slightly through the simulated cycle length to around 1010 kN in the calculated stiffness degradation of about 10-12%, which is slightly lower than that of M35. Displacement after unloading is low (approximately 0.6 mm), which confirms very high fatigue resistance and recovery of shape during cyclic loading at the service level.

On the other hand, the M40 slab without reinforcement has severe pinching and quick deterioration in stiffness during cyclical loading (Figure 13(b)). The loops of hysteresis become much narrower as the cycles get larger, indicating an irregular opening and unsuccessful closing of the crack. Peak reaction force decreases by about 25-28% and residual displacement approaches 2.0-2.4mm, which is evidence of cumulative damage and low fatigue performance.

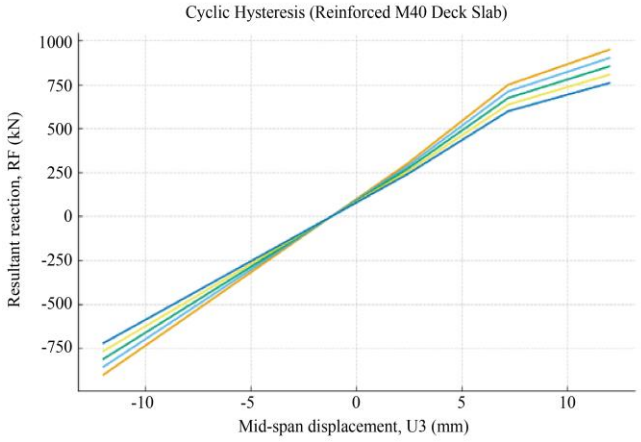

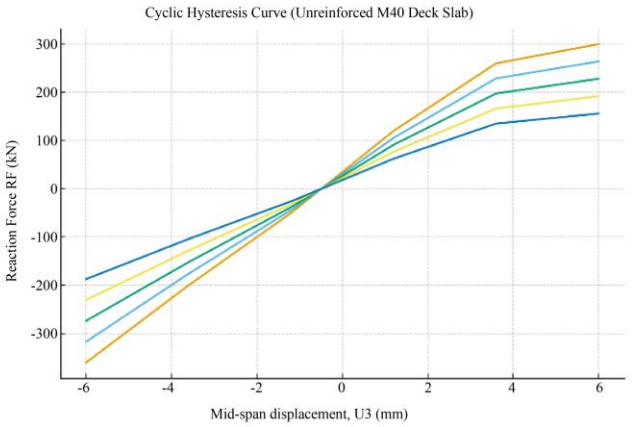

Fig. 13 (a) Cyclic hysteresis curves of GFRP-reinforced M40 deck slab, and (b) Cyclic hysteresis curves of unreinforced M40 deck slab.

4.3.3. Comparative Performance: Reinforced vs. Unreinforced (M40)

The statistical and cyclic RF-U3 outcomes (Figures 12(a) -13(b)) indicate the efficiency of GFRP reinforcement in enhancing the flexural capacity and fatigue life of M40 deck slabs. The reinforced slab is stiffer initially (185kN/mm vs. 170kN/mm), cracks later, and has much better load-carrying capacity and post-cracking behaviour. The reinforced system has symmetric hysteresis loops under cyclic loading with minimal stiffness degradation, but in contrast, the unreinforced slab behaves brittlely with extreme pinching, high rates of loss of stiffness, and high residual deformation. The key performance parameters were compared quantitatively as demonstrated in Figures 14(a)-c), revealing significant enhancement of cracking load, peak load, and ductility through the GFRP reinforcement. The ductility ratio rises from about 2.4 (unreinforced) to 6.3 (reinforced), which proves the change of brittle to semi-ductile behaviour that can be used during repetitive vehicular loading.

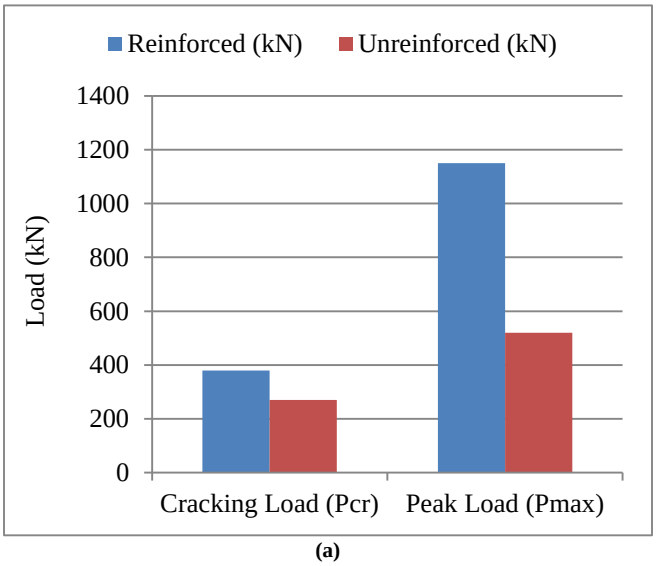

(a)

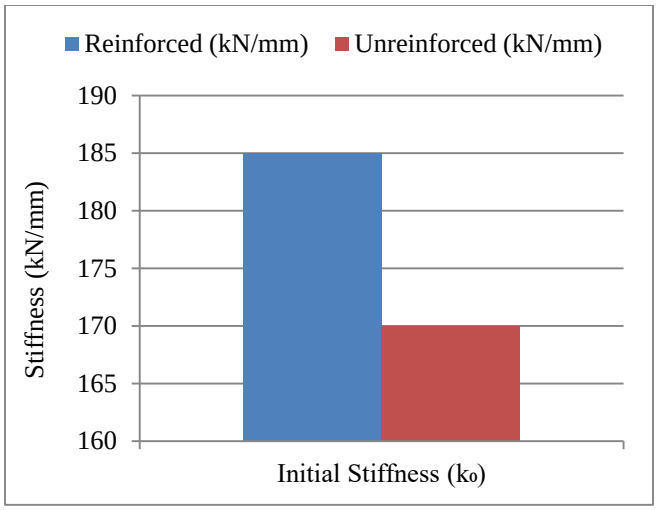

(b)

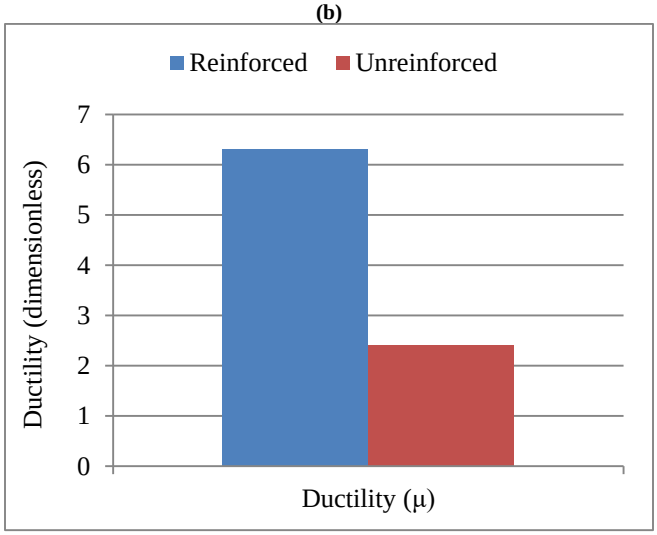

(c)

Fig. 14 (a) Comparison of cracking and peak loads (M40), (b) Comparison of initial stiffness k_0(M40), and (c) Comparison of ductility ratio μ (M40).

4.3.4. Summary of Load–Displacement Behaviour (M40)

The load displacement evaluation shows that GFRP reinforcement can contribute a lot to improving flexural strength, ductility, and cyclic stability of M40 concrete bridge deck slabs. Although the unreinforced slab has immediate cracking, sudden post-peak softening, and quick stiffness loss when subjected to cyclic loading, the reinforced slab shows steady hysteretic behaviour with few residual deformations. The high retention of stiffness and slow crack formation that was seen in the M40 slab in comparison to M35 further confirms the beneficial effect of increased concrete strength when working with a GFRP reinforcement on bridge deck applications that are re-exposed to service-level load.

4.4. Load–Displacement Response Comparison between M35 and M40 (Tabulated Evaluation)

A statistical comparison of the load-displacement properties of GFRP reinforced M35 and M40 deck slabs is

shown in Table 2. The parameters of stiffness, cracking resistance, strength, ductility, and cyclic performance obtained in the RF -U3 responses are compared.

Findings reveal that the first stiffness (ko) of the M40 slab slightly exceeds that of M35, indicating the high elasticity strength of the concrete with high strength. Greater enhancement is seen in the cracking load with about 15-18% improvement of M40, which validates the increase in tensile crack resistance. There is also an improvement of about 12-15% in the peak load capacity of the M40 slab, which proves to have better flexural strength without losing deformational capacity.

Although the strength is increased, the ductility ratio (μ) of the M40 slab is similar to M35, which means that the availability of the GFRP reinforcement has been able to eliminate brittle behaviour that is generally inherent with high-strength concrete. Cyclic loading has shown that M40 slabs are less susceptible to stiffness degradation (10-12%) and show a lower residual deflection value, which is indicative of better fatigue and stiffness retention. Both slabs have moderate characteristics of energy dissipation, which is controlled by micro-crack friction and crack closure instead of plastic yielding.

In general, as the tabulated comparison shows, the gains in the cracking resistance, load-carrying capacity, and cyclic durability of concrete increased by increasing the concrete grade to M40, but the post-cracking behaviour remains stable because of the successful GFRP reinforcement. This shows that concrete strength improvement does not substitute but complements (enhances) the value of reinforcement, thus both grades can be used to apply to bridge deck construction with regard to serviceability and structural durability goals.

Table 2. Comparison of M35 and M40

Parameter	M35 Reinforced	M40 Reinforced	Observation
Initial stiffness k_0 (kN/mm)	175	185	M40 shows ~6% higher elastic stiffness
Cracking load Pcr (kN)	360	420	≈15–18% improvement with M40 concrete
Deflection at cracking (mm)	2	1.8	Slightly reduced cracking deformation in M40
Peak load Pmax (kN)	1050	1180	≈12–15% higher peak capacity for M40
Deflection at peak (mm)	9	8.5	Comparable deformation capacity
Ductility ratio μ	6	6.4	Ductility is maintained despite higher strength
Cyclic stiffness degradation (%)	12–15%	10–12%	M40 exhibits better fatigue stiffness retention
Residual deflection after cycling (mm)	< 1.0	< 0.6	Improved recovery for M40 slab
Energy dissipation	Moderate	Moderate–High	Slight improvement due to delayed cracking
Failure mode	Controlled flexural cracking	Controlled flexural cracking	No brittle behaviour in either case

4.5. Stress and Damage Response of GFRP-Reinforced and Unreinforced Deck Slabs

This section presents a comparative discussion of the stress distribution and damage evolution in GFRP-reinforced and unreinforced concrete deck slabs of grades M35 and M40. The objective is to establish a mechanistic explanation for the load–displacement behaviour and cyclic performance trends discussed earlier in Sections 4.2–4.4, using representative contour responses obtained from the Concrete Damage Plasticity (CDP) simulations.

4.5.1. Stress Distribution under Static Loading

The von Mises stress distribution of the GFRP-reinforced M35 and M40 deck slabs under the static loading is presented in Figure 15. The stress values in the M35 slab are between 0.21 MPa and 2.53 MPa, with the highest stress being at the mid-span point of the patch load, which verifies flexural bending as the predominant response. The variation of the stress across the thickness of the slab is gradual, with the compression on the surface and the tension on the bottom fibre. The same stress pattern can be noticed in the M40 slab, wherein maximum von Mises stress of approximately 2.54 MPa is experienced at the level of the slabs, and less and less stress is observed as you move closer to the supports. M40 slab has been proven to exhibit a 12-15 percent lower peak stress intensity than M35, which implies an increased stiffness and more efficient load distribution. The highest stresses in both the slabs are much less than the compressive strength of the concrete, which is an important validation that the reaction is mostly elastic. Figure 15 is relevant in that it

confirms realistic stress transfer, consistent numerical behaviour, and an elastic baseline state before a build-up of damage and stiffness deterioration at cyclic loading.

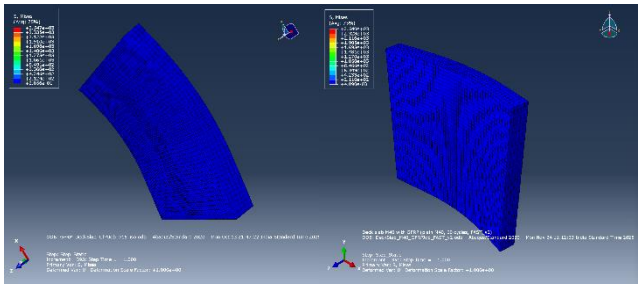

Fig. 15 Von Mises stress distribution in GFRP-reinforced deck slabs under static loading: (a) M35, and (b) M40.

4.5.2. Tensile Damage Evolution under Static Loading

The tensile damage contours of the Concrete Damaged Plasticity (CDP) model demonstrate the development and propagation of flexural cracking in the GFRP-reinforced deck slab during the process of static loading. The tensile damage variable (DAMAGET) shifts in a range between 0 (undamaged) and 1 (completely damaged), which is largely concentrated around the lowest centre point of the slab (where flexural tensile stresses are the largest) directly under the patch load applied. As seen in the contour scale, the highest values of tensile damage attain about 0.55-0.60 in the most highly strained area, which means that there is the creation of controlled micro-cracks instead of full tensile breakdown. The level of damage around the area is significantly lower (DAMAGET < 0.20), which proves that cracking is not widespread over the span of the slab. The progressive change of colour between blue and red indicates a gradual scale of damage, which is typical of steady crack propagation with flexural activity. The small size of the tensile damage and average intensity proves the efficiency of the embedded GFRP reinforcement in closing the cracks and the tensile strain accumulation suppression in the soffit. The reinforcement encourages micro-cracking that is evenly dispersed rather than sudden localization of cracks that lead to stiffness and brittle flexural fractures. Such a pattern of damage is directly linked to the stable post-cracking response and increased ductility in the static load-displacement behaviour.

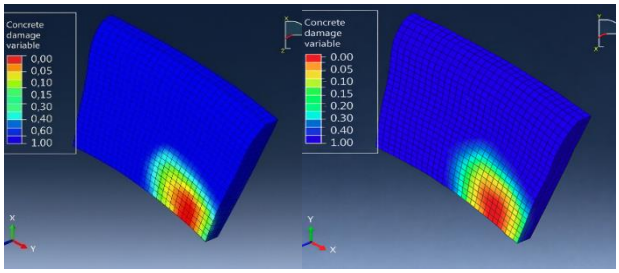

Fig. 16 Concrete tensile damage distribution (DAMAGET) in the GFRP-reinforced deck slab under static loading, showing localized flexural cracking near the soffit region beneath the applied patch load

4.5.3. Damage Response under Cyclic Loading

DAMAGET tensile damage contours under cyclic loading show that there is progressive accumulation of damage in the lower fibre area of the deck slab at the location of the applied patch load. As in the case of the M35 slab, the tensile damage variable takes values close to zero in the elastic regions, and maximum values of about 0.55-0.60 at the mid-span soffit upon entering the cyclic loading step. The damaged area is not widespread and does not expand extensively to the supports, which means that the growth of cracks is safe in the case of GFRP reinforcement.

In the case of the M40 slab, the same damage profile can be noticed, but the tensile damage peak is relatively lower and stays in the range of 0.45-0.50, which provides better crack resistance and stiffness with the increased concrete grade. Damage contours are less spatially dispersed and less intense than those of M35, which attests to slower damage development in repeated loading. Cyclic loading leads to greater levels of damage in both slabs compared to the situation during the static loading of the material because of the continuous opening and closing of the cracks. However, the lack of large areas of damage or abrupt localisation confirms that the GFRP-reinforced system has structural integrity in service-level cyclic loading. The development of damage as observed is comparable to the stable behaviour of hysteretic and low stiffness degradation of the load-displacement response.

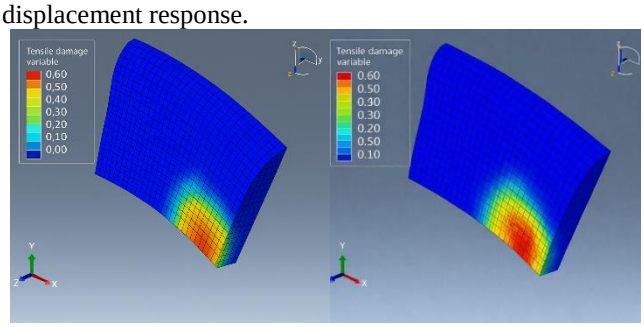

Fig. 17 Tensile damage contours (DAMAGET) under cyclic loading for (a) GFRP-reinforced M35 deck slab, and (b) GFRP-reinforced M40 deck slab, highlighting localized flexural damage near the soffit region beneath the loading patch.

4.5.4. Comparative Interpretation and Structural Implications

The integrated stress and damage behaviour proves that both GFRP-reinforced M35 and M40 deck slabs are flexure-dominated, and tensile cracking at the soffit controls the structural behaviour instead of compressive crushing or punching. M40 slab has a more homogeneous stress distribution and decreased stress concentration at the peaks in relation to M35, which indicates greater solidity and better load re- allocation. Tensile damage occurs earlier and spreads to a greater area in M35, as compared to the evolution of damage in M40, which is more localized and less severe during both static and cyclic loading. There is low compression damage in both slabs, showing that tensile

damage is the dominant degradation process. Structurally, these findings show that the use of GFRP reinforcement is effective in preventing localization of damage and increasing serviceability, and increasing concrete strength increases retention of stiffness and fatigue resistance in repeated loading.

4.6. Practical Design Recommendations

On the basis of the numerical findings of the current study, the following practical recommendations can be made for the design of GFRP-reinforced bridge deck slabs:

Concrete Grade Selection: Although M35 concrete meets service level strength and deflection requirements, increasing M35 to M40 offers quantifiable increases in cracking load (+16.7%), peak capacity (+12.4%), and cyclic stiffness retention (≈15-25% relative improvement). M40 concrete is therefore adopted in cases where bridge decks experience high traffic conditions, aggressive conditions, or fatigue-sensitive conditions.

4.6.1. Serviceability-Controlled Design

The slabs reinforced with the GFRP are flexural and serviceability-controlled, and the tensile damage and compressive crushing are localized. Design checks ought to be more focused on crack management and deflection limits as opposed to ultimate strength.

4.6.2. Fatigue and Cyclic Considerations

Lower residual deformation (<0.6 mm in M40 slabs) and reduced stiffness deterioration during repeated loading show that there is better elastic recovery. In bridges under a heavy load of traffic, a higher grade of concrete with GFRP reinforcement offers greater stability in terms of stiffness in the long run.

4.6.3. Ductility and Failure Mode

The ductility ratio was consistent (μ = 6-6.4), which demonstrated that an increment in the grade of concrete does not create brittle behaviour in the presence of GFRP reinforcement. This is in favour of safe adoption of increased strength of concrete without deteriorating deformation capacity.

4.6.4. Durability and Maintenance Perspective

With the corrosion resistance of GFRP reinforcement and better crack containment in higher-grade concrete, M40 GFRP-reinforced slabs can be used in coastal, de-icing salt, and high-humidity conditions where long-term durability is the determining performance factor.

4.7. Comparison with Codal Design Provisions for Validation and Benchmarking

The flexural, serviceability, and cyclic performance of the GFRP-reinforced bridge deck slabs were compared with corresponding design requirements in IS 456:2000, IRC 112:2020, ACI 440.1R, and CSA S806 to justify the numerical predictions. Indian codes make no direct mention of FRP reinforcement, so deflection and cracking limits were determined using the IS/IRC serviceability guidelines, and strength, ductility, and fatigue behaviour were determined based on the ACI/CSA guidelines on FRP-reinforced concrete members. The adopted slab geometry and layout of reinforcement were checked on codal limits, and numerical peak responses were compared with codal expectations of nonlinear finite element analysis (FEA) to determine the level of conservatism and applicability.

As noted in the comparison, both M35 and M40 GFRP-enhanced slabs are found to be in the codal serviceability range, the deflections are found to be within the service and 250 times the span criteria, and breakage is found to be outside the service load range. In comparison to M35, the M40 slab has an enhanced initial stiffness, delayed initiation of cracks, and enhanced fatigue stiffness retention with similar ductility, in line with ACI 440 and CSA S806 design intent. Numerical peak capacities under ultimate loading were found to exceed codal demand levels without changing the failure mode that is governed by flexure, and this confirmed sufficient safety margins. Generally, the codal benchmarking proves the validity of the numerical framework and that the achievement of serviceability and fatigue performance upgrade to M40 concrete without breaking codal requirements, hence proving its applicability in GFRP-reinforced bridge deck designs.

Table 3. Codal benchmarking of GFRP-reinforced bridge deck slabs (Numerical vs Codal intent)

Performance Aspect	Codal Reference	Codal Expectation	Numerical Observation (M35 → M40)	Interpretation
Service deflection	IS 456 / IRC 112	≤ Span/250	Within limit → Further reduced	Codally compliant
Cracking behaviour	ACI 440.1R	Controlled cracking acceptable	Delayed crack initiation in M40	Improved serviceability
Flexural strength	ACI 440 / CSA S806	≥ Factored demand	~12–15% higher capacity in M40	Enhanced safety margin
Failure mode	ACI 440.1R	Concrete-controlled failure	Flexure-controlled response	Codally acceptable
Ductility	CSA S806	Adequate deformation capacity	$\mu \approx 6.0 \rightarrow 6.4$	Maintained / improved
Fatigue performance	CSA S806	Limited stiffness degradation	Lower degradation and residual deflection in M40	Improved durability

4.8. Comparative Load–Displacement Performance of Steel- and GFRP-Reinforced Deck Slabs

Table 4 and Figure 18 show a benchmark of the load-displacement behaviour of plain concrete, steel-reinforced, and GFRP-reinforced bridge deck slabs. The steel-reinforced slab has increased ductility as a result of reinforcement yielding, but the GFRP-reinforced slab has increased cracking resistance, reduced residual deformation, and consistent post-cracking behaviour, which is controlled by elastic redistribution and concrete damage. Despite the slightly better peak load capacity of the steel-reinforced slabs, the GFRP-reinforced slab demonstrates better serviceability performance under repeated loads, such as lower stiffness degradation and better fatigue resistance. The findings suggest that GFRP reinforcement is an alternative to the traditional steel reinforcement that offers serviceability properties to bridge deck slabs that are exposed to traffic loading.

4.8.1. Interpretation of Steel-Reinforced Deck Slab Behaviour with Respect to Codal Provisions

The benchmark load displacement behaviour used in the steel-reinforced deck slab is aligned with the design philosophy of IRC 112 and IS 456, which permits tensile steel reinforcement yielding and other accompanying inelastic deformations as the acceptable mechanisms in ensuring ductility and redistribution of loads in reinforced concrete bridge decks. In this regard, the steel-reinforced slab shows that after cracking, the stiffness decreases, followed by a yielding-dominated behaviour, which increases the deformation capacity and significant residual deflection under cyclic conditions. This behaviour (with wider crack widths and irreversible deformations) is codal permissible in conventional RC slabs as long as overall structural safety is at risk, and thus is a realistic and code-consistent benchmark behaviour that can be compared with GFRP-reinforced deck slabs.

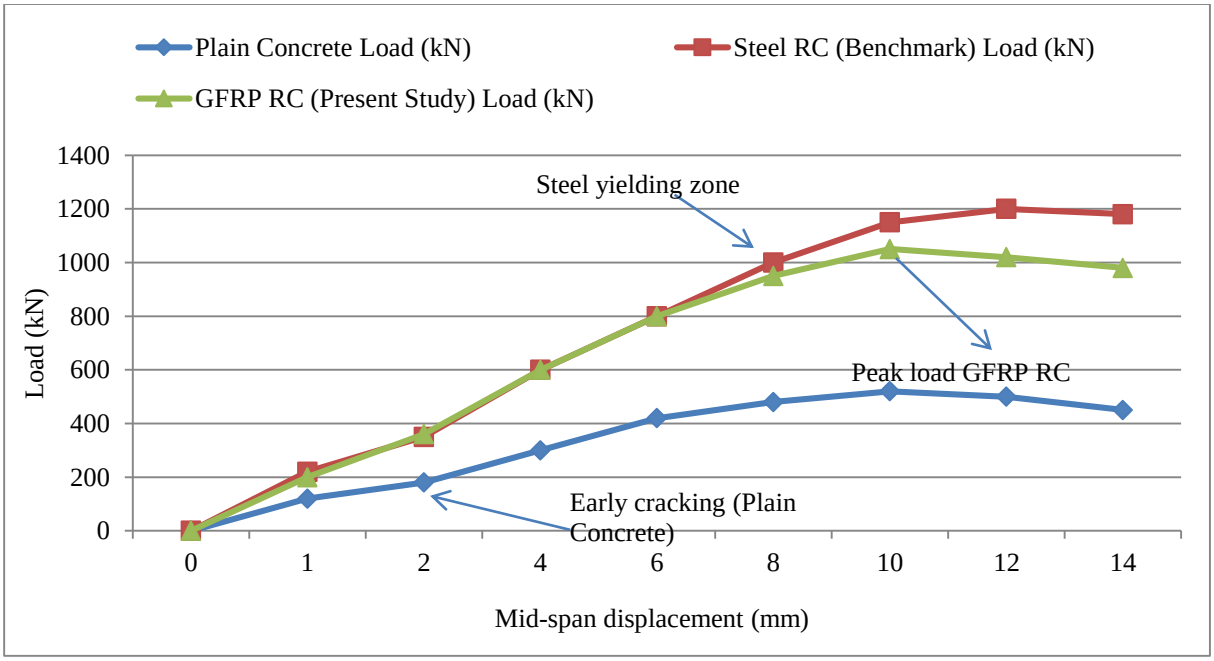

Fig. 18 Comparison of load–displacement response of plain concrete deck slab, steel-reinforced concrete deck slab (benchmark response based on literature), and GFRP-reinforced concrete deck slab (present numerical study), highlighting cracking, yielding, and peak load characteristics.

Table 4. Quantitative comparison of load–displacement performance of plain concrete, steel-reinforced (benchmark), and GFRP-reinforced (present study) bridge deck slabs under static and cyclic

Parameter	Plain Concrete Slab	Steel RC Slab (Benchmark)	GFRP RC Slab (Present Study)
Initial stiffness (kN/mm)	Low (~90)	High (~210)	Moderate–High (~175)
Cracking load Pcr (kN)	~180	~300	~360
Yield load Py (kN)	—	~720	—
Peak load Pmax (kN)	~520	~1200	~1050
Deflection at peak (mm)	~5.2	~14.5	~9.0
Post-cracking stiffness	Poor	Stable (yielding)	Stable (elastic redistribution)
Residual deflection	High	Moderate	Very low (<1 mm)
Governing behaviour	Brittle	Ductile (yielding)	Serviceability-controlled
Fatigue resistance	Poor	Good	Very good
Durability	High	Poor (corrosion-prone)	Excellent

4.9. Sensitivity Analysis of Key Variables

4.9.1. Sensitivity Definition and Calculation Procedure

A parametric sensitivity analysis (deterministic) was conducted by considering the concrete grade as the main parameter (M35 and M40) and keeping the geometry, reinforcement layout, boundary conditions, and loading protocols constant. The normalized sensitivity index was calculated as:

$$S_R(\%) = \frac{R_{M40} - R_{M35}}{R_{M35}} \times 100$$

In cases where the lower the response quantity, the better the performance (e.g., deflection and cyclic degradation), an improvement-based sensitivity was provided:

$$S_R(\%) = \frac{R_{M40} - R_{M35}}{R_{M35}} \times 100$$

Table 5. Sensitivity analysis table (M35 vs M40)

Response parameter	M35 value	M40 value	Units	Sensitivity definition	Sensitivity (%)	Interpretation	Notes
Initial stiffness k0	175	185	kN/mm	(M40−M35)/M35	5.714285714	Higher elastic stiffness	
Cracking load Pcr	360	420	kN	(M40−M35)/M35	16.66666667	Improved crack resistance	
Deflection at cracking	2	1.8	mm	(M35−M40)/M35 (lower better)	10	Lower cracking deformation	
Peak load Pmax	1050	1180	kN	(M40−M35)/M35	12.38095238	Higher peak capacity	
Deflection at peak	9	8.5	mm	(M35−M40)/M35 (lower better)	5.555555556	Reduced peak deformation	
Ductility ratio μ	6	6.4	-	(M40−M35)/M35	6.666666667	Ductility maintained/slightly improved	
Cyclic stiffness degradation (min case)	15	12	%	(M35−M40)/M35 (lower better)	20	Improved stiffness retention	Using M35=15%, M40=12%
Cyclic stiffness degradation (max case)	12	10	%	(M35−M40)/M35 (lower better)	16.66666667	Improved stiffness retention	Using M35=12%, M40=10%
Residual deflection after cycling (upper bound)	1	0.6	mm	(M35−M40)/M35 (lower better)	40	Improved elastic recovery	Using upper bounds (<1.0 mm, <0.6 mm)

4.9.2. Interpretation

The sensitivity analysis results suggest that the largest sensitivity of improvements in cracking load (+16.67) and the peak capacity (+12.38) is found in changing the concrete grade M35 to M40, indicating that concrete strength increases significantly in crack initiation resistance and load-carrying capacity when subjected to wheel-type loading.

The deformation measures related to serviceability (deflection at cracking and deflection at peak) improve moderately (5.56-10%), and ductility is preserved. The decrease in the stiffness degradation and residual deformation under cyclic loading confirms the enhancement in stiffness retention and elastic recovery, which is better related to serviceability in terms of fatigue.

4.10. Data Analysis, Error Quantification, and Fatigue Damage Assessment

4.10.1. Statistical Quantification of Performance Differences

The quantitative comparison of the grades of concrete (M35 and M40) and the reinforcement conditions (reinforced and unreinforced) was conducted in terms of percentage change values. Where R is the quantity of response obtained, the relative change was calculated as:

$$\Delta R(\%) = \frac{R_2 - R_1}{R_1} \times 100$$

In cases where the minimum score represents better performance (e.g., residual deflection, stiffness degradation), the improvement index was calculated as:

$$I_R(\%) = \frac{R_1 - R_2}{R_1} \times 100$$

The grade upgrade (M35 to M40) offered a noticeable effect on serviceability parameters: initial stiffness changed to 185 kN/mm (from 175, +5.71%), cracking load changed to 420 kN/mm (from 360, +16.67%), and peak load changed to 1180 kN/mm (from 1050, +12.38%). Peak deflection was lowered to 8.5 mm (Iδ ≈ 5.56%) and ductile behaviour retained (6.0-6.4, +6.67%). These findings show that concrete grade is the primary determinant of stiffness and crack initiation, with an equal deformation capacity.

4.10.2. Error Quantification and Numerical Consistency Checks

Numerical stability and credibility of the results were evaluated in terms of typical verification checks: (i) balance of reaction forces with the applied pressure load, (ii) coherence of linear load-displacement response before cracking, and (iii) steady development of damage and deformation without non-physical oscillation in the course of unloading/reloading. The smoothness and symmetry of reinforced slab hysteresis loops further assure convergent behaviour in the cyclic step. Such checks confirm the fact that reported trends of stiffness degradation and residual deformation are a response of the structure and not numerical artifacts.

4.10.3. Fatigue Damage Indices from Cyclic Response

The cyclic loading, being designed to reflect repeat actions of service-level traffic loads, was used to quantify fatigue behaviour by the response-based damage indices obtained as a result of FE.

(a) Stiffness degradation index

$$D_k(n) = \frac{k_0 - k_n}{k_0} \times 100$$

where k_0 is the start-up stiffness (Cycle 1) and k_n is the effective stiffness of a cycle n. The degree of degradation of the stiffness after 60 cycles was 12-15% in M35 and 10-12% in M40, meaning that the higher-grade slab had a better retention of the stiffness.

(b) Residual deflection index

$$D_\delta = \frac{\delta_r}{\delta_{max}}$$

Where δr is the residual (permanent) deflection following unloading, and δ_max is the maximum deflection. The reinforced slabs had extremely low residual deflection (<1.0 mm of M35 and <0.6 mm of M40), which attests to the improvement in elastic recovery and reduction of the permanent deflection at repeated loading.

(c) Concrete damage indices from CDP

The maximum variables of damage were monitored to describe the fatigue-related localization of damage:

$$D_t = \max(\text{DAMAGET}), D_c = \max(\text{DAMAGEC})$$

The contour distributions provide tensile damage concentration at the lower end of the loading area and compressive damage at negligible levels, in line with serviceability-regulated flexural behaviour.

4.10.4. Regression Fit for Stiffness Degradation vs Cycle Number

A logarithmic degradation model was used in order to give a compact analytical representation of the stiffness deterioration with the cycles:

$$D_k(n) = a\ln(n) + b$$

The general fatigue pattern of early rapid degradation and slow stabilization is represented by this model. Since not all cycles had intermediate cycle-wise stiffness values exported, the regression was fitted against restricted degradation trends in line with the terminal degradation ranges at 60 cycles. The fitted coefficients reveal that the range of M40 degrades more slowly than that of M35 (smaller a), which confirms the fact that the upgrading of the concrete grade decreases the dampening of the stiffness under the same cyclic loading.

4.10.5. S–N Curves and Future Fatigue-Life Extension

The current study measures fatigue performance at service load level using stiffness degradation, residual deformation, and CDP damage evolution under a limited-cycle procedure. To achieve a complete fatigue life prediction by stress-life (SN) based methods, reinforcement stress range – Δσat, at critical locations, and calibrated S-N relations are required to calculate cycles-to-failure Nf and cumulative damage (e.g., Miners rule). This extension is referred to as future work to facilitate the prediction of life considering variable-amplitude traffic loading.

4.11. Life-Cycle Assessment Considerations

The choice of reinforcement of bridge deck slabs has implications for the economic and environmental performance in the long term. A life-cycle assessment must be based on the production of materials, their construction, maintenance, and end-of-life, based on a specific functional unit and target service-life. Although steel reinforcement is cheaper at the start-up, it is prone to corrosion in areas that are exposed to chlorides, thus resulting in cracking, spalling, and frequent repair processes.

On the contrary, GFRP reinforcement will not have corrosion as the main form of deterioration, which may lead to fewer repairs and user disturbances during the service life.

Despite the fact that the current research is limited to structural response to the static and cyclic loads, enhanced crack control and decreased residual deformation of the GFRP-strengthened slabs suggest possible long-term serviceability advantages. A quantified environmental assessment and life-cycle cost will need project-specific inventory data and exposure conditions, which will be dealt with in future work by standardized life-cycle modelling.

5. Conclusion

This work numerically examined the performance of GFRP-reinforced concrete bridge deck slabs, both in the stationary and dynamic conditions, using nonlinear finite element analysis, including the effects of concrete grade (M35 and M40). Results indicate that there is an improvement in the initial stiffness of approximately 68%, the cracking load by 15-18%, and the peak load by 12-15% with the upgrade of the concrete grade to M40 rather than M35 under static loading conditions.

At cyclic loading, the M40 slab had less stiffness degradation (10-12%) and residual deflection (less than 0.6 mm) than the M35 slab, showing better fatigue resistance and elastic recovery. In both, the slabs met serviceability requirements and flexurally controlled behaviour with local tensile cracking and insignificant compression damage, which validated the functionality of GFRP reinforcement in bridge deck constructions that needed durability, corrosion resistance, and long-term serviceability.

Comparative evaluation indicates that improvements in the concrete grade of M35 to M40 offer measurable performance advantages (such as an increase in the initial stiffness of about 6-8%, an increase in the cracking load of about 15-18%, and an increase in peak load capacity of 12-15%). The strength was increased, but ductility remained (ductility ratio 6.0-6.4), and cyclic stiffness deterioration was minimized by about 2-3%, which is a sign of better fatigue capabilities.

Codal comparison to IS 456, IRC 112, ACI 440, and CSA S806 was used to verify that the two slabs are compliant with codal intent, with M40 slabs having higher safety and serviceability margins. These results justify the logical use of M40 concrete in GFRP-reinforced bridge deck slabs that are subjected to the same repeated traffic load.

A benchmark comparison with steel-reinforced bridge deck slabs indicates that GFRP-reinforced slabs achieve comparable strength with superior serviceability performance, reduced residual deformation, and enhanced durability under cyclic loading. This confirms the suitability of GFRP reinforcement as a long-term alternative to steel for bridge deck applications governed by repeated traffic loads.

5.1. Long-Term Durability Considerations

The resistance to environmental exposure and long-term cyclic loading is the key to the long-term performance of bridge deck slabs. GFRP bars, unlike steel reinforcement, do not undergo electrochemical corrosion, and this minimizes the cracking and loss of stiffness that is caused by corrosion-induced expansion. Structurally, durability has a close relationship with crack control, retention of stiffness, and residual deformation during repeated traffic load.

The current nonlinear analysis exhibited stable localization of cracks, constrained compressive damage, and controlled reduction of stiffness in the presence of cyclic loads. The lower residual deflection and high stiffness retention at the concrete grade higher point signify better elastic recovery and better fatigue performance, factors that will favour long-term serviceability.

The model currently used presumes material properties are fixed and does not actively represent the effects of an environment (moisture diffusion, temperature change, creep, shrinkage, or bond degradation) on a material. In the future, time-dependent and environment-dependent material models can be extended to facilitate performance-based service life prediction.

5.2. Limitations and Future Research Recommendations

Despite the elaborate nonlinear finite element analysis presented in the current study, there are various areas of concern that need to be explored further:

5.2.1. Experimental Validation

To check trends of stiffness degradation and evolution of damages as predicted in the numerical model, full-scale experimental testing under static and high-cycle loads is required.

5.2.2. Bond–Slip Behaviour

The existing model presupposes the presence of a perfect bond with embedded constraints. The interface constitutive modelling should be included in future research so as to simulate bond degradation when subjected to fatigue loading.

5.2.3. The Environmental and Time-Dependent Effect

Coupled durability-mechanical modelling should be implemented in order to evaluate life-cycle behaviour through long-term exposure to moisture, temperature variation, and chemical attack.

5.2.4. Fatigue Life Prediction (S-N Framework)

Reinforcement stress ranges that will be extracted and calibrated S-N relationships will facilitate cumulative predictions of fatigue life with the use of damage accumulation models.

5.2.5. Probabilistic Design and Reliability-Based Design

Probabilistic modelling should be used to include parametric uncertainty in material properties, magnitude of loading, and environmental exposure in order to come up with reliability-based design guidelines.

5.2.6. Life-Cycle Assessment and Cost Optimization

It should be suggested that a quantified life cycle cost and environmental impact analysis, with consideration of maintenance frequency and service life extension, would be used to support infrastructure-level decision-making.

References

[1] Tarek Alkhrdaj et al., "Guide for the Design and Construction of Structural Concrete Reinforced with FRP Bars," *Proceedings*, American Concrete Institute, Farmington Hills, MI, USA, pp. 1-44, 2006. [Google Scholar]

[2] CSA Group, "CSA S806-12: Design and Construction of Building Structures with Fibre-Reinforced Polymers," *Canada: Canadian Standards Association*, 2012. [Google Scholar] [Publisher Link]

[3] LAASHTO, "AASHTO LRFD Bridge Design Guide Specifications for GFRP-Reinforced Concrete," *American Association of State Highway and Transportation Officials (AASHTO)*, Washington, DC, USA, 2018. [Google Scholar] [Publisher Link]

[4] B. Fib, "FRP Reinforcement in RC Structures," *Desing and use of Fibre Reinforced Polymer Reinforcement (FRP) in Reinforced Con-Crete Structures*, 2007. [Google Scholar]

[5] Ehab El-Salakawy et al., "Field Investigation on the First Bridge Deck Slab Reinforced with Glass FRP Bars Constructed in Canada," *Journal of Composites for Construction*, vol. 9, no. 6, pp. 470-479, 2005. [CrossRef] [Google Scholar] [Publisher Link]

[6] Brahim Benmokrane et al., "Designing and Testing of Concrete Bridge Decks Reinforced with Glass FRP Bars," *Journal of Bridge Engineering*, vol. 11, no. 2, pp. 217-229, 2006. [CrossRef] [Google Scholar] [Publisher Link]

[7] Amr El-Ragaby, Ehab El-Salakawy, and Brahim Benmokrane, "Fatigue Analysis of Concrete Bridge Deck Slabs Reinforced with E-Glass/Vinyl Ester FRP Reinforcing Bars," *Composites Part B: Engineering*, vol. 38, no. 5-6, pp. 703-711, 2007. [CrossRef] [Google Scholar] [Publisher Link]

[8] Valter Carvelli, Marco Andrea Pisani, and Carlo Poggi, "Fatigue Behaviour of Concrete Bridge Deck Slabs Reinforced with GFRP Bars," *Composites Part B: Engineering*, vol. 41, no. 7, pp. 560-567, 2010. [CrossRef] [Google Scholar] [Publisher Link]

[9] American Concrete Institute. Committee 440, "Guide for the Design and Construction of Structural Concrete Reinforced with FRP Bars: ACI 440.1R-06," American Concrete Institute, 2006. [Google Scholar]

[10] Fareed Elgabbas, Ehab A. Ahmed, and Brahim Benmokrane, "Experimental Testing of Concrete Bridge-Deck Slabs Reinforced with Basalt-FRP Reinforcing Bars Under Concentrated Loads," *Journal of Bridge Engineering*, vol. 21, no. 7, pp. 1-16, 2016. [CrossRef] [Google Scholar] [Publisher Link]

[11] Minkwan Ju, Kyoungsoo Park, and Cheolwoo Park, "Punching Shear Behavior of Two-Way Concrete Slabs Reinforced with Glass-Fiber-Reinforced Polymer Bars," *Polymers*, vol. 10, no. 8, pp. 1-15, 2018. [CrossRef] [Google Scholar] [Publisher Link]

[12] Jacob Lubliner et al., "A Plastic-Damage Model for Concrete," *International Journal of Solids and Structures*, vol. 25, no. 3, pp. 299-326, 1989. [CrossRef] [Google Scholar] [Publisher Link]

[13] Jeeho Lee, and Gregory L. Fenves, "Plastic-Damage Model for Cyclic Loading of Concrete Structures," *Journal of Engineering Mechanics*, vol. 124, no. 8, pp. 892-900, 1998. [CrossRef] [Google Scholar] [Publisher Link]

[14] Chongxi Gao, and Amir Fam, "Fatigue Behavior under Rolling Load of a Full-Scale Bridge Deck with a Steel-Reinforced Section," *Journal of Bridge Engineering*, vol. 29, no. 12, 2024. [CrossRef] [Google Scholar] [Publisher Link]

[15] Yahia M.S. Ali et al., "Static and Fatigue Behavior of Concrete Bridge Deck Slabs Reinforced with Hybrid BFRP and Steel Bars," *Structures*, vol. 65, 2024. [CrossRef] [Google Scholar] [Publisher Link]

[16] Katie Chu, Khandaker Muhammed Anwar Hossain, and M. Lachemi, "Fatigue Behaviour of Joint-Free Bridges with Steel and GFRP-Reinforced ECC Link Slabs," *Structures*, vol. 47, pp. 829-845, 2023. [CrossRef] [Google Scholar] [Publisher Link]

[17] Reza Hassanli et al., "Cyclic Behavior of GFRP-Reinforced Concrete One-Way Slabs with Synthetic Fibres," *Journal of Building Engineering*, vol. 65, 2023. [CrossRef] [Google Scholar] [Publisher Link]

[18] Thanongsak Imjai et al., "Serviceability Behaviour of FRP-Reinforced Slatted Slabs Made of High-Content Recycled Aggregate Concrete," *Structures*, vol. 51, pp. 1071-1082, 2023. [CrossRef] [Google Scholar] [Publisher Link]

[19] Bodena S. Negeo, "Numerical Validation on Post-Fire Performance of GFRP SIP Formwork for Concrete Bridge Decks at High Temperature," *Discover Civil Engineering*, vol. 2, no. 1, pp. 1-21, 2025. [CrossRef] [Google Scholar] [Publisher Link]

[20] Rajai Z. Al-Rousan, Mohammad Alhassan, and Razan Al-wadi, "Nonlinear Finite Element Analysis of Full-Scale Concrete Bridge Deck Slabs Reinforced with FRP Bars," *Structures*, vol. 27, pp. 1820-1831, 2020. [CrossRef] [Google Scholar] [Publisher Link]